http://dx.doi.org/10.5012/bkcs.2011.32.10.3660

CO-Tolerant PtMo/C Fuel Cell Catalyst for H_2 Oxidation

Jin Ho Bang[*] and Hasuck Kim[†,*]

Department of Chemistry and Applied Chemistry, Hanyang University, Ansan 426-791, Korea. [*]E-mail: jbang@hanyang.ac.kr
[†]Department of Energy System Engineering, Daegu Gyeongbuk Institute of Science & Technology (DGIST), Daegu 700-742, Korea. [*]E-mail: hasuckim@dgist.ac.kr
Received July 10, 2011, Accepted August 15, 2011

CO-tolerant PtMo/C alloy electrocatalyst was prepared by a colloidal method, and its electrocatalytic activity toward CO oxidation was investigated. Electrochemical study revealed that the alloy catalyst significantly enhanced catalytic activity toward the electro-oxidation of CO compared to Pt/C counterpart. Cyclic voltammetry suggested that Mo plays an important role in promoting CO electro-oxidation by facilitating the formation of active oxygen species. The effect of Mo on the electronic structure of Pt was investigated using X-ray absorption spectroscopy to elucidate the synergetic effect of alloying. Our in-depth spectroscopic analysis revealed that CO is less strongly adsorbed on PtMo/C catalyst than on Pt/C catalyst due to the modulation of the electronic structure of Pt d-band. Our investigation shows that the enhanced CO electro-oxidation in PtMo alloy electrocatalyst is originated from two factors; one comes from the facile formation of active oxygen species, and the other from the weak interaction between Pt and CO.

Key Words : Fuel cell, PtMo electrocatalyst, CO electro-oxidation, H_2 oxidation, X-ray absorption spectroscopy

Introduction

Fuel cell is an electrochemical device which can continuously convert the chemical energy of fuel and oxidant to electrical energy through redox reactions. Because of their high-energy conversion efficiency and low pollutant emission, the feasibility of fuel cells has long been examined for diverse applications. Various types of fuel cells have been developed, including phosphoric acid fuel cell (PAFC), proton exchange membrane fuel cell (PEMFC), direct methanol fuel cell (DMFC), and solid oxide fuel cell (SOFC).[1] Among them, PEMFC has been extensively investigated as part of an effort to develop an alternative power source for vehicles.[2] In the operation of PEMFC, hydrogen gas (H_2) is supplied to anode as a fuel. In general, H_2 is produced by converting methanol using a reformer.[3] One of the problems associated with the reformer is that the reaction often ends incomplete, leaving small amounts of carbon monoxide (< 1%) behind in H_2. Carbon monoxide (CO), however, is extremely poisonous to fuel cell catalyst: even a few parts per million of CO substantially deteriorates the performance of fuel cell.[4,5] One approach to solve this problem is to selectively oxidize CO to CO_2 in the reformer using an extra reactor, but the requirement of such additional system is not cost-effective and makes the reformer system more complicated. Another approach is utilizing platinum alloy catalysts which have a low susceptibility to CO poisoning but maintains a high kinetic rate for H_2 oxidation. A wide variety of Pt-based alloy catalysts have been investigated and the research is well-summarized in literatures.[4,6] Typically, transition metals such as ruthenium, tin, tungsten, or molybdenum have been utilized as a component of the alloys,[7-18] and among them ruthenium (Ru) has received great attention due to the significant improvement in the anodic oxidation of CO with PtRu catalyst.[7,19-22] Watanabe and coworkers proposed a bifunctional mechanism to explain such enhancement of catalytic activity, where Ru promotes the adsorption of active oxygen species which plays a critical role in the electro-oxidation of CO.[21] Along with Ru, molybdenum (Mo) has attracted scientists' interest because of their relatively lower cost as well as the catalytic activity of PtMo comparable to that of PtRu. Grgur and coworkers reported that the magnitude of H_2 oxidation current with the PtMo catalyst in low-overpotential region is nearly the same as that observed with the PtRu catalyst.[9,23,24] Most importantly, PtMo requires less overpotential for CO electro-oxidation by ~0.15 V.[24,25] Despite the disparate chemical properties of Ru and Mo, the characteristics of PtMo catalyst appear to be similar to those of PtRu catalyst, thus the enhancement induced by Mo was generally ascribed to the bifunctional mechanism. The role of Mo in CO electro-oxidation, however, remains elusive. Like in the case of PtSn and PtNi catalysts,[12,26,27] one cannot completely exclude a possibility that the modulation of electronic structure induced by Mo could have an effect on the interaction of Pt and CO, which also dictates the catalytic activity. To elucidate the alloying effect on the adsorption strength of CO, we investigated the role of Mo in CO electro-oxidation using X-ray absorption spectroscopy, and our results are discussed.

Experimental

Synthesis of PtMo Electrocatalyst. PtMo electrocatalyst supported on a carbon black was prepared by adapting the colloidal method originally developed for the preparation of PtRu catalyst by Bönnemann and coworkers.[28] All experi-

Table 1. XRD and EDS data analysis

Catalyst	Atomic composition/ Pt:Mo		Lattice parameter (Å)	Particle size[a] (nm)
	As-prepared	EDS		
Pt/C (E-TEK)	-	-	3.928	3.1
Pt_4Mo_1/C (15 min)	80 : 20	81 : 19	3.921	3.5
Pt_4Mo_1/C (30 min)	80 : 20	79 : 21	3.923	3.6
Pt_4Mo_1/C (45 min)	80 : 20	79 : 21	3.927	3.5

[a]The particle size calculated from XRD analysis.

ments were carried out with dry solvents under nitrogen atmosphere. The reducing agent used in this synthesis, tetraoctylammonium triethylhydroborate ($NOct_4[BEt_3H]$), was synthesized by mixing tetraoctylammonium bromide ($NOct_4Br$) and potassium triethylhydroborate ($K[BEt_3H]$) in tetrahydrofuran (THF). $NOct_4[BEt_3H]$ in THF was then added dropwise to the solution of anhydrous $PtCl_2$ and $MoCl_5$ in THF under vigorous stir at 40 °C, and the resulting solution was left stirred for 16 hours to complete the reaction. The synthesized PtMo nanoparticles dispersed in THF were mixed with a carbon black (Vulcan XC-72, Cabot) dispersed in THF, and the suspension was stirred for a day to allow the complete adsorption of the nanoparticles on Vulcan XC-72. The prepared electrocatalyst was filtered, rinsed thoroughly with excess ethanol and water several times, and dried under air. Finally, the catalyst was annealed at 300 °C under the atmosphere of 10% O_2 in N_2 for 15, 30, and 45 minutes, respectively, to remove any residual organic species. The metal loading in the catalyst was 20 weight % (wt %), and the atomic ratio of Pt to Mo was set to 4:1, which was confirmed by elemental analysis (Table 1). The resulting catalysts will hereafter be referred to as Pt_4Mo_1/C (15 min), Pt_4Mo_1/C (30 min), and Pt_4Mo_1/C (45 min), respectively.

Characterization. X-ray diffraction patterns were obtained with a CN2115 diffractometer (Rigaku) with nickel-filtered Cu K_α radiation. The chemical composition of PtMo alloy catalysts was analyzed using an energy-dispersive X-ray detector (Oxford, QX-2000) attached to the electron probe X-ray microanalysis (EPMA, JEOL JXA-8900R). Transmission electron microscopy (TEM) images were taken using a JEM-200CX electron microscope at an accelerating voltage of 200 kV.

Electrochemical Measurements. All electrochemical experiments were performed in a standard three-electrode jacketed cell with an electrochemical analyzer (BAS 100B/W, Bioanalytical Systems). The working electrode was fabricated by casting a compact thin layer of catalytic powder mixed with Nafion (5 wt % in mixture of lower aliphatic alcohols and water, Aldrich) onto glassy carbon electrode (GC-20S, Tokai Carbon Co., Ltd. 3 mm diameter) as reported previously.[29] The resulting layer was then rinsed with water and immersed in 1 M H_2SO_4 solution for 12 hours prior to measurements. The potential of the working electrode was measured with Ag/AgCl electrode as a reference electrode, but all potentials in this work were reported with respect to the normal hydrogen electrode (NHE) potential. The counter electrode was a platinum wire, and the temperature of electrolyte was controlled using a LAUDA Model 20 constant temperature circulator. Cyclic voltammetry was performed at a scan rate of 50 mV/s in 1 M H_2SO_4 electrolyte, which was purged with nitrogen gas (N_2) before measurements. For CO-stripping voltammetry, CO was adsorbed to the catalysts by applying external potential (0.1 V *vs.* NHE) in CO-saturated 1 M H_2SO_4 solution for 3 minutes. After CO had been completely expelled from the electrolyte by bubbling N_2, potentials were swept at a rate of 10 mV/s. In order to evaluate the electrocatalytic activity toward H_2 oxidation, rotating disk electrode (RDE) measurements were conducted. For complete CO poisoning, CO was adsorbed to working electrode at 0.1V *vs.* NHE in CO-saturated 1 M H_2SO_4 solution for 3 min, and the remaining CO was expelled from the electrolyte by bubbling N_2. The electrode was subsequently rotated at 2500 rounds per minute (rpm) and the potentials were swept at a rate of 1 mV/s. During the measurement, H_2 containing 0.1% CO, denoted as 0.1% CO/H_2, was continuously purged through the electrolyte to ensure H_2-saturated condition.

X-ray Absorption Spectroscopy. X-ray absorption spectra were recorded with a X-ray fluorescence detector at the Pohang Accelerator Laboratory (PAL) using the beam line 7C operated at 2.5 GeV and 90-140 mA. A Si (111) double flat crystal with an energy resolution ($\Delta\lambda/\lambda$) of 2.0×10^{-14} at 10 keV was employed as a monochromator. For CO adsorption experiments, X-ray absorption spectrum of each electrocatalyst was taken before and after being exposed to CO gas. For CO adsorption, the electrocatalysts were exposed to CO gas for 30 minutes to ensure the complete coverage of CO on the surface. *In-situ* XAS experiments were carried out in 1.0 M H_2SO_4 at room temperature. Working electrodes were prepared by applying the catalyst paste mixed with polytetrafluoroethylene (PTFE) onto carbon paper as described in our report,[30] and Ag/AgCl and Pt wire were used as reference and counter electrode, respectively. X-ray absorption spectra were recorded before and after CO adsorption. CO was adsorbed in the same way as described above. After CO was removed by CO-stripping voltammetry, the absorption spectra were taken again. The potential control and recording data during the *in-situ* experiment were carried out using a potentiostat (PAR 273 potentiostat, EG&G PARC) and an X-Y recorder (Kipp & Zonen), respectively.

Results and Discussion

XRD patterns of Pt_4Mo_1/C alloy electrocatalyst were analyzed to examine structural change when platinum was alloyed with molybdenum. Figure 1 shows the XRD patterns of three Pt_4Mo_1/C alloy catalysts which were heat-treated for different times, and the diffraction patterns are compared with that of Pt/C (E-TEK, 20 wt %). There are no noticeable changes in the diffraction patterns of Pt_4Mo_1/C when compared with Pt/C, suggesting that the alloy catalysts preserve Pt lattice structure with a similar lattice parameter (Table 1). The average particle size of each catalyst was determined

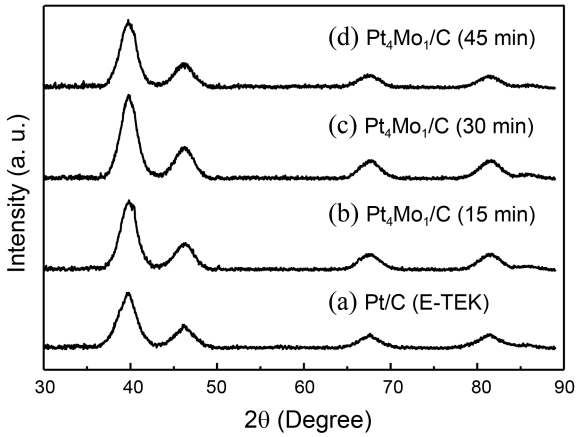

Figure 1. XRD patterns of (a) Pt/C (E-TEK) and (b-d) Pt_4Mo_1/C annealed for 15, 30, 45 mins, respectively.

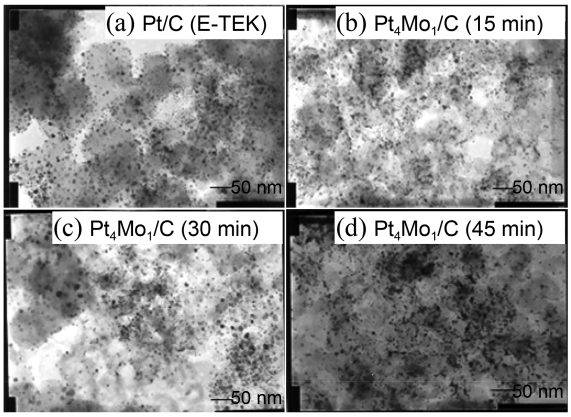

Figure 2. TEM micrographs of (a) Pt/C (E-TEK) and (b-d) Pt_4Mo_1/C annealed for 15, 30, 45 mins, respectively.

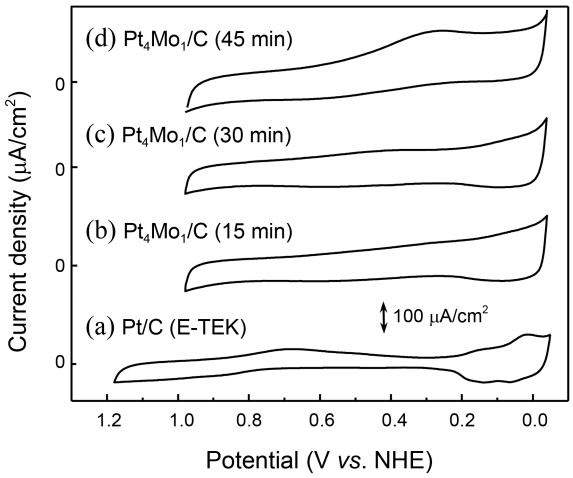

Figure 3. Cyclic voltammograms of (a) Pt/C (E-TEK) and (b-d) Pt_4Mo_1/C annealed for 15, 30, 45 mins, respectively (electrolyte: 1 M H_2SO_4, scan rate: 50 mV/s, temperature: 20 °C).

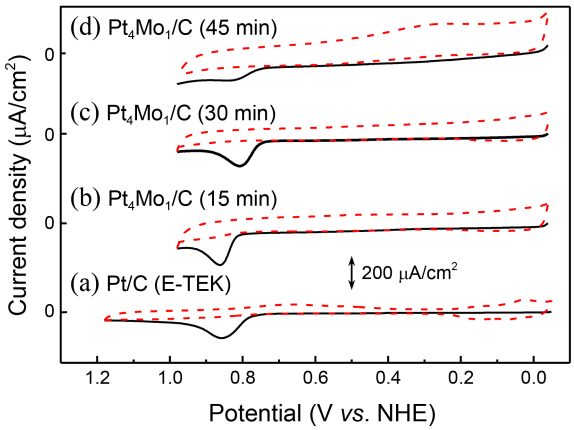

Figure 4. CO-stripping voltammograms of (a) Pt/C (E-TEK) and (b-d) Pt_4Mo_1/C annealed for 15, 30, 45 mins, respectively (electrolyte: 1 M H_2SO_4, scan rate: 10 mV/s, CO adsorption at 0.1 V for 3 minutes). Note that red, dashed lines represent the cylic voltammogram of each catalyst in the absence of CO.

from the broadening of the (111) peak using the Debye-Sherrer equation, and the particle sizes of the catalyst are calculated to be 3-4 nm (Table 1). The distribution of the metal particles on the carbon support in Pt_4Mo_1/C and Pt/C was examined by TEM analysis. The dispersion of particles in all the catalysts appears homogeneous in general, but small agglomerates of alloy particles are sporadically observed in Pt_4Mo_1/C catalysts (Figure 2). Particle size ranges from 2.5 to 4 nm, which is in good agreement with our calculation obtained by the XRD analysis.

Cyclic voltammetry was performed to characterize the surface properties of catalysts. Figure 3 shows the cyclic voltammograms of three Pt_4Mo_1/C catalysts and Pt/C in 1 M H_2SO_4 electrolyte. Unlike Pt/C catalyst, which shows distinct peaks for hydrogen adsorption and desorption, all Pt_4Mo_1/C catalysts exhibit large double-layer capacitance throughout the entire potential region. This pseudocapacitive feature is attributed to the formation of OH species on Mo atoms on the surface of alloy particles.[23] The nature of the oxidation states of Mo surface atoms, however, is still obscure and not clearly resolved, but the investigation by Mukerjee and coworkers suggested that the oxyhydroxide state of Mo, predominantly as $MoO(OH)_2$, is responsible for the oxidative removal of CO.[25] Another noticeable change in the cyclic voltammograms of Pt_4Mo_1/C catalysts is that the double-layer area becomes thicker as the annealing time increases. This implies that more Mo atoms were diffused out to the surface of alloy particles as the annealing under oxygen atmosphere was prolonged.

CO-stripping voltammetry is a simple, effective method to compare the activity of electrocatalyst toward the electro-oxidation of CO. Figure 4 displays the CO-stripping voltammograms of Pt/C and Pt_4Mo_1/C catalysts, in which the oxidation currents observed in all the catalysts peaked at similar potentials (0.8-0.9 V). The most positive peak potential was observed in Pt_4Mo_1/C (30 min), which is more positive than that of Pt/C by 0.05 V. This implies that Pt_4Mo_1/C is superior to Pt/C for CO electro-oxidation, which is attributed to more efficient removal of CO by the assistance of active oxygen species formed on Mo. As the annealing was prolonged for additional 15 minutes, how-

ever, the peak moved back to more negative potential, and the entire peak area of CO oxidation was also significantly decreased. We speculate that the heat-treatment under oxygen atmosphere promoted the movement of Mo atoms to the surface of alloy particles, thus the number of Pt surface atoms for CO adsorption was dramatically decreased. The increase in Mo surface atoms with annealing time is in fact consistent with our observation in cyclic voltammetry. On the basis of our electrochemical study, Pt_4Mo_1/C (30 min) turns out to be the most optimized catalyst in our current study, thus we hereafter use only this catalyst for further investigation.

Despite the usefulness of CO-stripping voltammetry in the evaluation of CO-tolerance, it fails to provide a direct evidence of CO oxidation in low potential region (0.05-0.6 V). To examine the CO oxidation in this potential region, potentiodynamic oxidation experiment using rotating disk electrode was performed. An advantage of this measurement is its ability of simulating the continuous flow conditions encountered in the real operation of PEMFC.[19,20] Figure 5 shows the potentiodynamic oxidation of 0.1% CO/H_2 on Pt/C and Pt_4Mo_1/C alloy catalyst in 1 M H_2SO_4 at 60 °C. In order to assure the equilibrium of CO adsorption, CO was adsorbed at 0.1 V for 3 minutes prior to recording the oxidation current. The magnitude of the oxidation current with Pt_4Mo_1/C catalyst in the low potential region was much greater than that with Pt/C. This results from more effective removal of CO on the surface of Pt_4Mo_1/C catalyst as confirmed by CO-stripping voltammetry; Pt_4Mo_1/C is capable of providing more free Pt reaction sites for H_2 electro-oxidation. This observation therefore demonstrates that our Pt_4Mo_1/C catalyst indeed oxidizes CO more effectively than Pt/C even with lower overpotentials.

There has been much debate on the role of Mo in the improved catalytic activity. As discussed above, the bifunctional mechanism has been proposed to explain the enhancement. This argument has been partly supported by several observations. For instance, spectroscopic analysis revealed that Mo surface atoms have active oxygen species at all potentials, which may act as a promoter for the oxidization of adsorbed CO on neighboring Pt atoms.[9,23,25] While the bifunctional mechanism sounds plausible as in the case of PtRu alloy catalyst, one cannot completely exclude another possible reason for the improved CO-tolerance: the adsorption strength of CO on Pt atoms. If CO molecules are less tightly bound to the surface of Pt, the removal of CO would be much easier and do not require high overpotentials for the oxidation.

CO adsorption on Pt has been described by the donation-retrodonation model originally proposed by Blyholder.[31] According to this model, the adsorption of CO results from two simultaneous bond stabilization effects; one induced by the electron transfer from the 5σ-orbital of CO to the d-band of Pt, and the other from the retrodonation of electrons to the π* (or 2π) antibonding orbitals of CO. Anderson and coworkers revealed earlier that the strength of CO bonding to Pt is predominantly determined by the degree of stabilization of the 5σ orbital.[32] Since this stabilization is due to the mixing of the 5σ orbital with Pt d-band, the investigation of d-band structure of Pt (*i.e.*, Pt d-band vacancy) may provide an insight into the adsorption strength of CO on Pt.

In our study, X-ray absorption spectroscopy (XAS) was performed to examine the interaction of CO with Pt. A powerful aspect of the analysis of X-ray absorption near edge structure (XANES) lies in its capability of providing useful information on changes in the electronic structure of Pt-based alloy catalysts.[33-36] Typically, the Pt d-band vacancy is derived from the analysis of Pt L_{III} edge, which is created by the excitation of $2p_{3/2}$ electrons to empty states in the vicinity of Fermi level. The change in the Pt L_{III} peak is normally interpreted as the variation in Pt d-band vacancy:

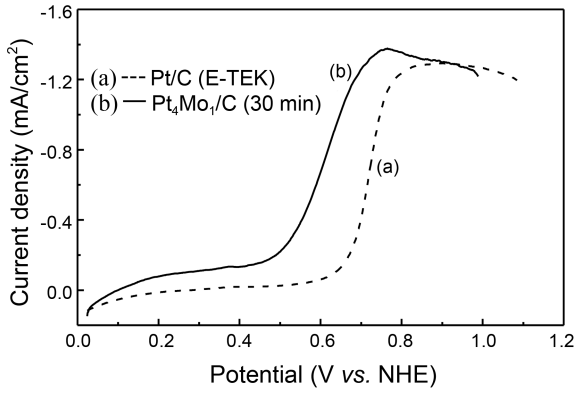

Figure 5. Potentiodynamic oxidation of 0.1% CO/H_2 on (a) Pt/C (E-TEK) and (b) Pt_4Mo_1/C (30 min). Electrolyte: 1 M H_2SO_4, scan rate: 1 mV/s, rotating speed: 2500 rpm, temperature: 20 °C.

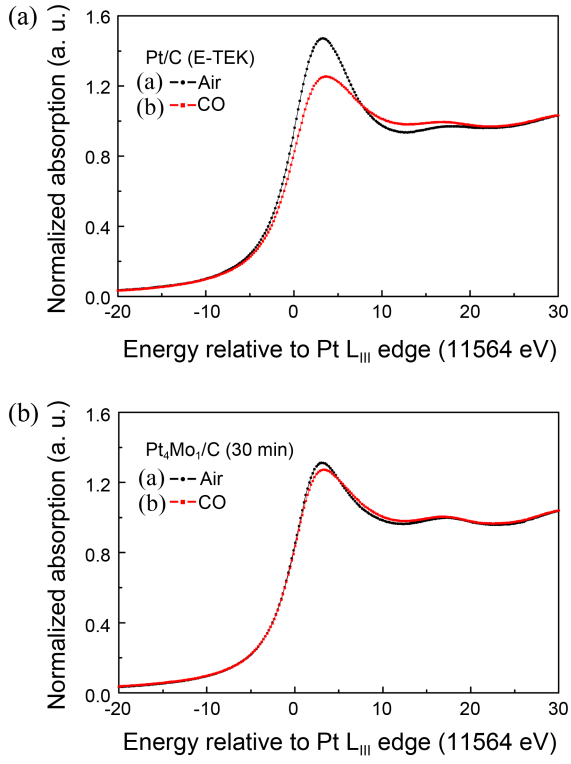

Figure 6. Gas-phase XANES spectra of (A) Pt/C (E-TEK) and (B) Pt_4Mo_1/C (30 min) (a) before and (b) after CO adsorption.

the intensity of Pt L_{III} peak varies proportionally with the increase in Pt d-band vacancy.[33] This therefore allows us to monitor the adsorption strength of CO.

Figure 6 shows the Pt L_{III}-edge XANES spectra of Pt/C and Pt_4Mo_1/C before and after CO adsorption. The XANES spectra of each catalyst obtained prior to CO adsorption exhibited that the peak intensity at the Pt L_{III}-edge was significantly reduced in Pt_4Mo_1/C, indicating that the alloying indeed affects the d-band structure of Pt. After the catalysts were poisoned with CO, the d-band structure of Pt in each catalyst was examined again. A noticeable change after CO adsorption was the reduced intensity of the absorption maxima, which results from the charge transfer from the highest occupied CO orbital (5σ) to empty d orbitals on Pt atoms. This change appears much more dramatic in Pt/C than in Pt_4Mo_1/C, implying that more electrons are transferred to the d-band of Pt in the case of Pt/C. Since this σ donation strengthens Pt-CO bond, this observation suggests that CO is more strongly adsorbed on Pt/C than on Pt_4Mo_1/C.

In spite of the usefulness of the gas-phase XAS experiment, the information on the interaction between Pt and CO is somewhat limited because the environment under which the experiment was conducted is distinctly different from the real condition encountered during fuel cell operation. To address such limitation, we designed *in-situ* XAS experiment where the catalysts were in contact with a liquid electrolyte. Figure 7 shows the XANES spectra of Pt/C and Pt_4Mo_1/C before and after they were poisoned with CO in 1 M H_2SO_4. Both catalysts showed the decrease in the peak intensity after CO adsorption as observed in the gas-phase experiment. The variation in the intensity, however, is much smaller than that observed in the gas-phase experiment. We speculate that this is intimately associated with the complexity of Pt-CO interaction in aqueous solution, which is created by the simultaneous presence of water molecules at the surface of catalysts. In our *in-situ* experiment, CO was removed by linear sweep voltammetry and XANES spectra were subsequently recorded to examine the recovery of d-band vacancy induced by the CO desorption. The recovery of d-band vacancy is closely related to the ease of CO desorption. Therefore, as suggested by the gas-phase XAS experiment, if the interaction between Pt and CO is weaker in Pt_4Mo_1/C, CO could be easily removed from Pt_4Mo_1/C than from Pt/C. This would lead to the increase in the peak intensity in the XAS experiment. As we expected, the absorption maximum barely changed in the case of Pt/C, indicating that a fairly large amounts of CO are still adsorbed on Pt. In the case of Pt_4Mo_1/C, however, the intensity of absorption peak rose, implying that a considerable number of CO molecules became released from the surface of Pt_4Mo_1/C. The *in-situ* XANES analysis therefore proves our hypothesis that Mo modulates the electronic structure of Pt such that CO molecules are less tightly bound to Pt_4Mo_1/C than to Pt/C. Our present study suggests that this weaker interaction between Pt and CO induced by alloying performs an important function in CO electro-oxidation, along with the active oxygen species on Mo. A comprehensive study is currently underway to get more insight into this intriguing alloying effect.

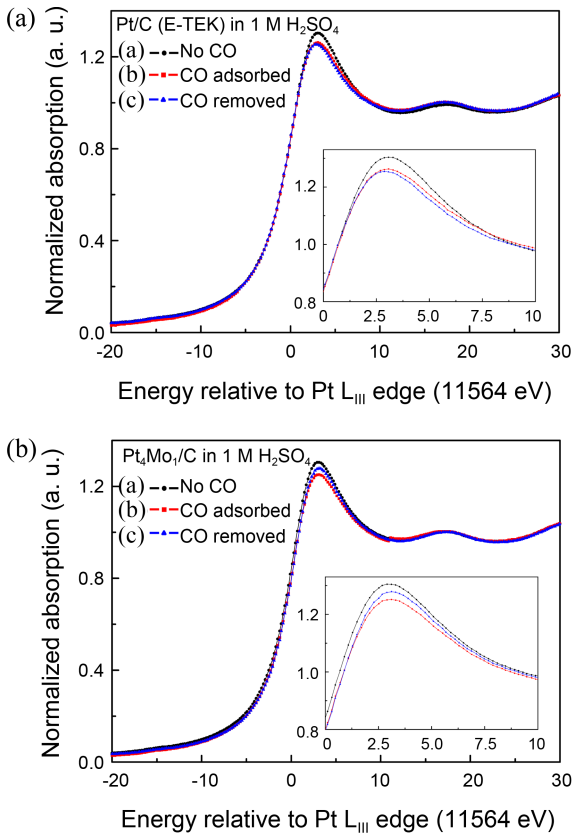

Figure 7. *In-situ* XANES spectra of (A) Pt/C (E-TEK) and (B) Pt_4Mo_1/C (30 min) in 1 M H_2SO_4 (a) before CO adsorption, (b) after CO adsorption, and (c) after CO stripping voltammetry, respectively (insets: close-ups of the spectra at Pt L_{III} absorption edge).

Conclusions

Carbon-supported Pt_4Mo_1 alloy electrocatalysts were explored as a CO-tolerant electrocatalyst for H_2 oxidation. Electrochemical measurements revealed that Pt_4Mo_1/C is more active for CO electro-oxidation than non-alloyed Pt/C catalyst. The role of Mo in promoting the CO electro-oxidation was investigated in this study. Cyclic voltammetry combined with CO-stripping voltammetry show that the improved activity results from the facile formation of active oxygen species on Mo at lower overpotentials, which is consistent with the argument based on the bifunctional mechanism. Effect of Mo on the adsorption strength of CO on the alloy catalyst was examined using X-ray absorption spectroscopy. Our in-depth study revealed that Mo modulates the d-band of Pt, resulting in weaker adsorption of CO on Pt_4Mo_1/C than on Pt/C. On the basis of our observation, we conclude that along with the bifunctional mechanism where Mo acts as a source of active oxygen species, the weak Pt-CO interaction induced by alloying with Mo plays a critical role in the enhanced catalytic activity toward CO oxidation.

Acknowledgments. This work was supported by the research fund of Hanyang University (HY-2010-N).

References

1. Sundmacher, K. *Ind. Eng. Chem. Res.* **2010**, *49*, 10159-10182.
2. Wagner, F. T.; Lakshmanan, B.; Mathias, M. F. *J. Phys. Chem. Lett.* **2010**, *1*, 2204-2219.
3. Palo, D. R.; Dagle, R. A.; Holladay, J. D. *Chem. Rev.* **2007**, *107*, 3992-4021.
4. Igarashi, H.; Fujino, T.; Watanabe, M. *J. Electroanal. Chem.* **1995**, *391*, 119-123.
5. Markoviæ, N. M.; Grgur, B. N.; Lucas, C. A.; Ross, P. N. *J. Phys. Chem. B* **1999**, *103*, 487-495.
6. Antolini, E. *Mater. Chem. Phys.* **2003**, *78*, 563-573.
7. Gasteiger, H. A.; Markovic, N.; Ross, P. N.; Cairns, E. J. *J. Phys. Chem.* **1994**, *98*, 617-625.
8. Gasteiger, H. A.; Markovic, N. M.; Ross, P. N. *J. Phys. Chem.* **1995**, *99*, 8945-8949.
9. Grgur, B. N.; Markovic, N. M.; Ross, P. N. *J. Phys. Chem. B* **1998**, *102*, 2494-2501.
10. Liu, Z.; Hu, J. E.; Wang, Q.; Gaskell, K.; Frenkel, A. I.; Jackson, G. S.; Eichhorn, B. *J. Am. Chem. Soc.* **2009**, *131*, 6924-6925.
11. Morimoto, Y.; Yeager, E. B. *J. Electroanal. Chem.* **1998**, *441*, 77-81.
12. Mu, R.; Fu, Q.; Xu, H.; Zhang, H.; Huang, Y.; Jiang, Z.; Zhang, S.; Tan, D.; Bao, X. *J. Am. Chem. Soc.* **2011**, *133*, 1978-1986.
13. Shim, J.; Lee, C.-R.; Lee, H.-K.; Lee, J.-S.; Cairns, E. J. *J. Power Sources* **2001**, *102*, 172-177.
14. Yano, H.; Ono, C.; Shiroishi, H.; Okada, T. *Chem. Commun.* **2005**, 1212-1214.
15. Liang, Y.; Zhang, H.; Tian, Z.; Zhu, X.; Wang, X.; Yi, B. *J. Phys. Chem. B* **2006**, *110*, 7828-7834.
16. Martinez-Huerta, M. V.; Rodriguez, J. L.; Tsiouvaras, N.; Peña, M. A.; Fierro, J. L. G.; Pastor, E. *Chem. Mater.* **2008**, *20*, 4249-4259.
17. Wang, D.; Subban, C. V.; Wang, H.; Rus, E.; DiSalvo, F. J.; Abruña, H. D. *J. Am. Chem. Soc.* **2010**, *132*, 10218-10220.
18. Yamazaki, S.-I.; Yao, M.; Siroma, Z.; Ioroi, T.; Yasuda, K. *J. Phys. Chem. C* **2010**, *114*, 21856-21860.
19. Gasteiger, H. A.; Markovic, N. M.; Ross, P. N. *J. Phys. Chem.* **1995**, *99*, 16757-16767.
20. Gasteiger, H. A.; Markovic, N. M.; Ross, P. N. *J. Phys. Chem.* **1995**, *99*, 8290-8301.
21. Watanabe, M.; Motoo, S. *J. Electroanal. Chem.* **1975**, *60*, 275-283.
22. Bang, J. H.; Han, K.; Skrabalak, S. E.; Kim, H.; Suslick, K. S. *J. Phys. Chem. C* **2007**, *111*, 10959-10964.
23. Grgur, B. N.; Markovic, N. M.; Ross, P. N. *J. Electrochem. Soc.* **1999**, *146*, 1613-1619.
24. Grgur, B. N.; Zhuang, G.; Markovic, N. M.; Ross, P. N. *J. Phys. Chem. B* **1997**, *101*, 3910-3913.
25. Mukerjee, S.; Lee, S. J.; Ticianelli, E. A.; McBreen, J.; Grgur, B. N.; Markovic, N. M.; Ross, P. N.; Giallombardo, J. R.; De Castro, E. S. *Electrochem. Solid-State Lett.* **1999**, *2*, 12-15.
26. Mukerjee, S.; McBreen, J. *J. Electrochem. Soc.* **1999**, *146*, 600-606.
27. Dupont, C.; Jugnet, Y.; Loffreda, D. *J. Am. Chem. Soc.* **2006**, *128*, 9129-9136.
28. Schmidt, T. J.; Noeske, M.; Gasteiger, H. A.; Behm, R. J.; Britz, P.; Bönnemann, H. *J. Electrochem. Soc.* **1998**, *145*, 925-931.
29. Lawson, D. R.; Whiteley, L. D.; Martin, C. R.; Szentirmay, M. N.; Song, J. I. *J. Electrochem. Soc.* **1988**, *135*, 2247-2253.
30. Min, M.-K.; Cho, J.; Cho, K.; Kim, H. *Electrochim. Acta* **2000**, *45*, 4211-4217.
31. Blyholder, G. *J. Phys. Chem.* **1964**, *68*, 2772-2777.
32. Ray, N. K.; Anderson, A. B. *Sur. Sci.* **1982**, *119*, 35-45.
33. Russell, A. E.; Rose, A. *Chem. Rev.* **2004**, *104*, 4613-4636.
34. Alayoglu, S.; Zavalij, P.; Eichhorn, B.; Wang, Q.; Frenkel, A. I.; Chupas, P. *ACS Nano* **2009**, *3*, 3127-3137.
35. Mcbreen, J.; Mukerjee, S. *J. Electrochem. Soc.* **1995**, *142*, 3399-3404.
36. Mukerjee, S.; Urian, R. C. *Electrochim. Acta* **2002**, *47*, 3219-3231.